paper presented on 1998 Spring MRS Symposium on Microelectromechanical Structures

ADHESION OF POLYSILICON MICROBEAMS IN CONTROLLED HUMIDITY AMBIENTS

M. P. de Boer[1], P. J. Clews[2], B. K. Smith[2] and T. A. Michalske[3]
Sandia National Laboratories, Albuquerque, NM 87185

[1]Dept. 1325, Intelligent Micromachining, mpdebo@sandia.gov
[2]Dept. 1324, Silicon Processing
[3]Dept. 1114, Surface and Interface Science
www.mdl.sandia.gov/Micromachine

ABSTRACT

We characterize *in-situ* the adhesion of surface micromachined polysilicon beams subject to controlled humidity ambients. Beams were freed by supercritical CO_2 drying. Consistent adhesion results were obtained using a post-treatment in an oxygen plasma which rendered the microbeams uniformly hydrophilic. Individual beam deformations were measured by optical interferometry after equilibration at a given relative humidity (RH). Validation of each adhesion measurement was accomplished by comparing the deformations with elasticity theory. The data indicates that adhesion increases exponentially with RH from 30% to 95%, with values from 1 mJ/m^2 to 50 mJ/m^2. Using the Kelvin equation, we show that the data should be independent of RH if a smooth interface is considered. By modeling a rough interface consistent with atomic force microscopy (AFM) data, the exponential trend is satisfactorily explained.

INTRODUCTION

Adhesion (e.g., stiction) is a major concern in Microelectromechanical Systems (MEMS) reliability. MEMS devices are inherently sensitive to adhesion because the polycrystalline (poly) structural members are relatively compliant and only a few microns above the substrate. If a compliant member is brought into contact with the substrate by capillary, electrostatic or inertial forces, surface forces may cause the member to remain adhered after the external force is removed. The problem can occur during the final step of the manufacturing process. The devices, encased in glass, are "released" in HF acid, transferred to water, and then dried. Capillary forces are negative due to the surface tension of water on the wetted poly surface, and cause the beams to be pulled in to the substrate. Adhesion on the order of 10-100 mJ/m^2 is measured [1-5] .

Many methods have been investigated to overcome this initial problem [6-14] resulting in initially free beams. Supercritical CO_2 ($SCCO_2$) drying has been shown to free long cantilever beams [14] . Devices are transferred from water to methanol, and placed in a pressure vessel. In our laboratory, we pressurize with gaseous CO_2 in the vessel until the supercritical state is attained, and then displace the methanol [15] with $SCCO_2$. Supercritical CO_2 is subsequently vented, leaving beams up to 2 mm in length free.

While initially free devices greatly improve yield, structural members may still come into contact while in use due to electrostatic or inertial forces. Their adhesion then may depend greatly on the environment they are subject to. A key concern is the dependence of adhesion on relative humidity (RH), because water may eventually penetrate even hermetically sealed devices. If the operating temperature of the device drops, RH levels can increase towards 100% because of the exponential dependence of RH on water content. After supercritical drying, adhesion of about 10 μJ/m^2 and 140 mJ/m^2 has been measured using an activation pad near the support post at an RH of about 30% and 100% respectively [16]. However, these were not equilibrium values. It is important to measure the equilibrium performance of MEMS devices subject to various humidity ambients so that worst case behavior is known for design considerations.

EXPERIMENTAL

Test devices are polysilicon beams with an activation pad located near the support post, similar to ref. [16]. A cross-section of a beam is represented in Fig. 1. In this configuration, the

DISCLAIMER

beams and the landing are electrically connected at the end of the beam array (not shown) such that any interaction between the beam and the landing pad is adhesive only. We take a fracture mechanics perspective [4, 5, 17] in which s is the crack length, and the attached length d must be of substantial length, $\geq 0.05\,L$, where L is the beam length. The height of the support post is h and the beam thickness is t. The Young's Modulus E of the beams is assumed to be 170 GPa.

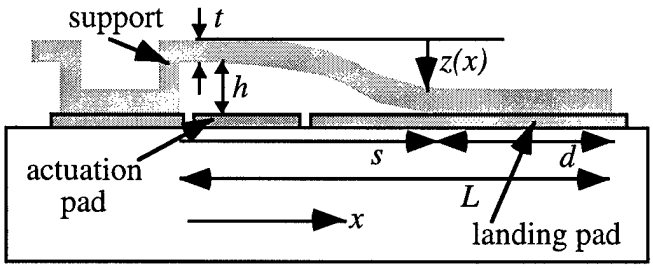

Fig. 1 Cross-section of beam geometry

The devices were fabricated at Sandia National Laboratories in the SUMMiT process [18]. The landing pad has a thickness of 0.3 μm. Its roughness after fabrication was measured by AFM to be 2.1 nm (rms). A sacrificial layer of thickness h=1.8 μm was deposited next. The poly beam is a thickness t of 2.25 μm, as measured by optical interferometry on a WYKO multiple wavelength device. The roughness on the bottom of the poly 2 was 2.4 nm (rms). The devices are subjected to a 1100 °C anneal to minimize residual stress as well as strain gradient. The devices are released in 1:1 HF:HCl for 90 minutes, transferred to water and then to hydrogen peroxide to obtain a thin (~1 nm) layer of SiO_2 on all poly surfaces. The devices were subsequently transferred to water, methanol and then supercritically dried.

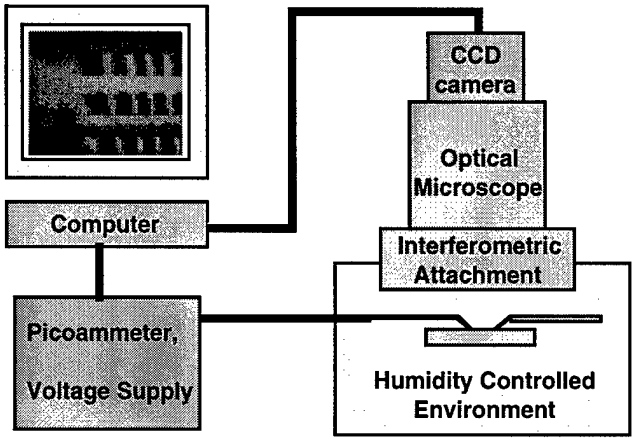

Fig. 2 Environmental Interferometric Microprober

In order to measure adhesion *in-situ*, we have constructed an Environmental Interferometric Microprobing Station, as represented in Fig. 2. Humidified nitrogen, introduced by bubbling through water, is mixed with dry nitrogen to control humidity. The humidity level is monitored by a Vaisala HMP234 humidity probe. The chamber is placed immediately under an optical microscope objective to which an interferometric attachment has been fixed. Tilt on the attachment is adjusted such that fringes on the substrate are parallel to the beams. In this fashion, fringes on the beams indicate out-of-plane (z) deflections. A latex seal between the chamber and the interferometric attachment isolates the chamber from the outside world. Image information is acquired by means of a CCD camera on the microscope. Image capture and RH monitoring is controlled by LabView [19] . By taking a linescan along a given beam using NIH Image [20], fringe information is digitized, and converted to z deflections by a computer program.

Adhesion is measured on each individual beam according to the following procedure. First, the beam must be adhered over a long length d, as seen in Fig. 1. Second, the deflections are normalized and compared to the equation [1]

$$z(x) = -h(3\eta^2 - \eta^3), \tag{1}$$

where $\eta = x / s$. Third, if agreement with Eq. (1) is good, then adhesion Γ (in J/m^2) is calculated according to

$$\Gamma = \frac{3}{2} E \frac{h^2 t^3}{s^4}. \tag{2}$$

We have found this methodology to be an improved method of adhesion measurement relative to measuring the shortest adhered beam in an array of beams [4, 5]. The reasons are (1) the deflection measurement validates the value for each beam, (2) the incremental area is well known, (3) the energy well is very deep, and (4) each beam gives a value for adhesion. The radius of curvature of free beams, as measured by interferometry, was 2.2 m, corresponding to 230 nm out of plane deflection for a 1000 μm long beam. Considering that these beams are nearly flat, curvature has a negligible effect on strain energy, and is ignored in the adhesion calculations.

RESULTS AND DISCUSSION

Adhesion results were erratic when samples were tested as-received from the supercritical drying apparatus. That is, pull-in behavior of the beams versus RH was different for each beam, even after a few days exposure time. We noticed that while test samples were fully wetted by water before entering the apparatus (i.e., a contact angle with water of ≤10°), the test samples had much higher contact angles (40-70°) after the supercritical drying procedure. Apparently the apparatus deposits a thin contamination film which increases the contact angle. While in general the contamination reduces adhesion at high RH, the erratic results indicate that the process is not controllable. The source of the contamination has been traced to the input pump, and cannot immediately be fixed. In order to alleviate this problem, samples were placed in an oxygen asher after the supercritical drying. Beams remained free, and on test samples the contact angle was again reduced to ≤10°. We conclude that the contamination layer is organic and removable by oxygen plasma, apparently leaving a well hydroxlyated surface which adsorbs water [21].

The beams were first placed in a 0% RH ambient for at least 16 hours to minimize water adsorbed from the ambient. Next, the beams are pulled into contact with the substrate via the activation pad. Because the beams are 1000 μm long, the beams remain in contact with the substrate over a long length d, and crack lengths are on the order of 600-850 μm, corresponding to Γ=68-17 μJ/m^2 respectively. Next, the RH was increased to 30%, and crack length s began to decrease, due to capillary action at the crack tip. After 40 hours, no further decrease was observed. RH was then increased to 45, 55, 70 and 95%. At each RH, equilibrium was attained for s within 24-40 hours before increasing to the next RH.

With the oxygen ashing after supercritical drying, the results were now much more consistent, as evidenced in Fig. 3. Here a uniform decrease in s was observed as RH was increased. At RH=30% after 40 hours as in Fig. 3a, the equilibrium length for most beams is about 350 μm. At this RH, one beam continues to have very long lengths s. We take this to be due to a local barrier preventing pull-in, perhaps due to local roughness being larger. However, at RH=45%, all beams displayed nearly the same length, indicating that such a barrier is small and is overwhelmed by the capillary forces as RH increases.

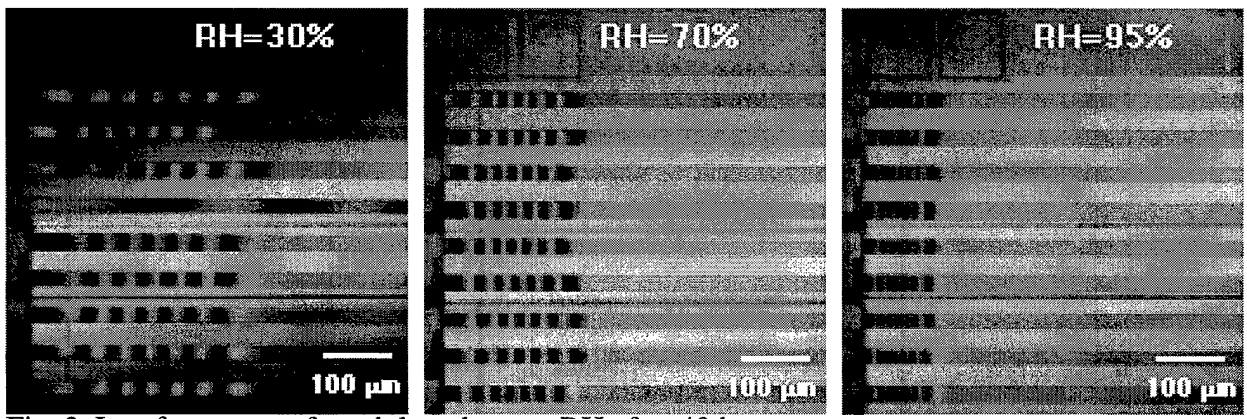

Fig. 3 Interferograms of crack length s vs. RH after 40 hours exposure.

An example of validation of the adhesion measurement is given in Fig. 4. Here, the linescan from an individual beam is plotted vs. position on the right hand ordinate for an individual

beam from Fig. 3a. This data is converted to z deflection vs. position data by a computer program, which is plotted on the left hand ordinate as a solid line. The dashed line represents Eq. (1). Because the data and the dashed line virtually overlap, the calculation of adhesion according to Eq. (2) is valid. In this case, the value of Γ is 0.5 mJ/m^2. This validation and measurement procedure was repeated for each of five beams at the five different RH values ranging from 30 to 95%, and is plotted in Fig. 5 (as indicated by "Data"), where each line represents an individual beam at different RH values. We see that the dependence of adhesion on RH is exponential.

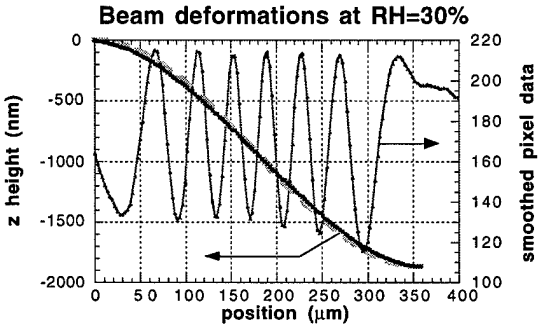

Fig. 4 z -deflections of an individual beam

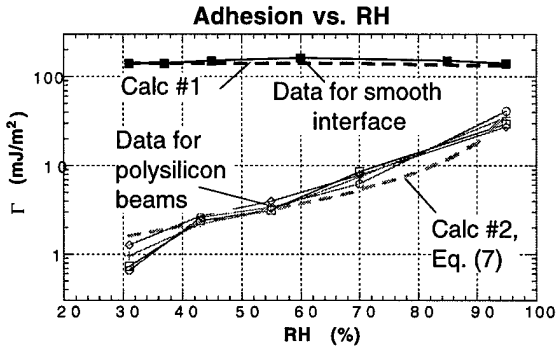

Fig. 5 Data and calculations

The Kelvin equation predicts the radius of a capillary in a narrow channel as a function of RH. We investigated two possibilities for how the Kelvin equation might explain our results. In the first model, we assume that the interface between the beams is smooth, such that a microcapillary extends across the width of the beam at the crack tip and exerts a tensile pressure according to the Laplace equation. This is schematically represented in Fig. 6. The radius of the capillary and the tensile force it exerts are then [22]

$$r_K = \frac{1.04}{\ln(\mathrm{RH})} \ \text{nm} \qquad (3) \qquad \text{and} \qquad q = \frac{2\gamma\cos\theta}{r_K} = \frac{0.142}{r_K} \ \frac{\mathrm{N}}{\mathrm{m}^2} \qquad (4).$$

Here, r_K is the Kelvin radius in nm, γ=71 mJ/m^2 is the surface tension of water and θ=0° for this hydrophilic sample is the contact angle of water with the surface. In Eq. (3), room temperature and atmospheric pressure are assumed. Using beam theory, we can calculate the deflections of a beam subject to the boundary conditions of 0 slope at the two ends, and a distributed force per unit area q exerted at one end. Defining the length from the support post to the beginning of the capillary drop as $s_1 = s - s_2$, the deflection for $0 \le x \le s_1$ is

$$z(x) = -\frac{1}{D}\left\{P\left(\frac{(s_1+s_2)x^2}{2} - \frac{x^3}{6}\right) - qs_2\left[\left(s_1 + \frac{s_2}{2}\right)\frac{x^2}{2} - \frac{x^3}{6}\right]\right\} \qquad (5a)$$

The stiffness modulus D is $Et^3/12$, and s_2, P and q are as in Fig. 6. P is a reaction force per unit width which develops in response to the capillary pressure at the crack tip. For $s_1 \le x \le s$,

$$z(x) = -\frac{1}{D}\left\{P\left(\frac{(s_1+s_2)x^2}{2} - \frac{x^3}{6}\right) - \frac{q}{2}\left[\frac{(s_1+s_2)^2x^2}{2} + \frac{x^4}{12} - \frac{(s_1+s_2)x^3}{3} - \frac{s_1^3x}{3} + \frac{s_1^4}{12}\right]\right\}. \qquad (5b)$$

Because r_K is small, the length s_2 over which it exerts force q is short (on the order of a micron). Therefore, Eq. (5) is virtually indistinguishable from Eq. (1) when the values of P and q are properly chosen. Iteration on s_1 and s_2, with a total deflection of h, is required to match the

values of r_K and q at a given RH from Eqs. (3) and (4). This was done using at RH values of 30, 70 and 95%. The result is that the sum $s_1 + s_2 = s$ is ~90 μm and is virtually independent of RH. This balance in s is because as RH increases, r_K increases, which increases s_2 but reduces q.

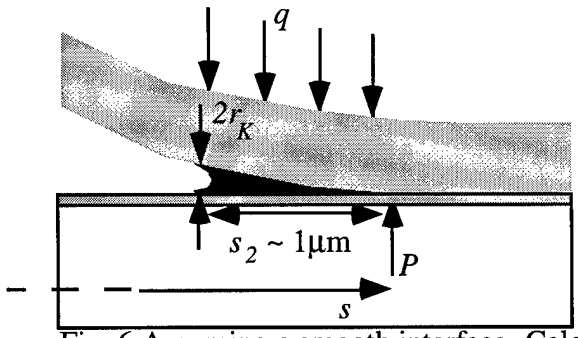

Fig. 6 Assuming a smooth interface- Calc #1

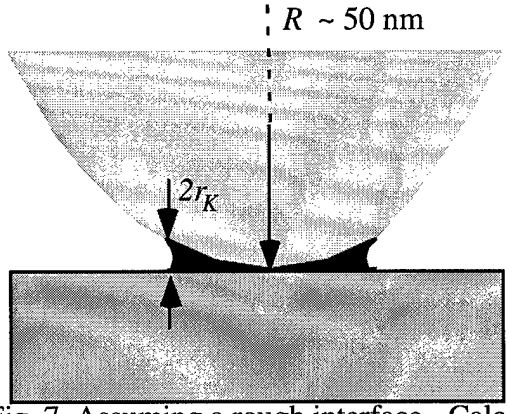

Fig. 7 Assuming a rough interface - Calc #2

Because the form of Eq. (5) is indistinguishable from Eq. (1), Eq. (3) may be used to calculate the effective Γ. For a smooth interface, the calculation shows that Γ should be 2γ=142 mJ/m^2, and independent of RH. This verifies that the expected value of $\Gamma=2\gamma$ from thermodynamic considerations is also a direct result of the mechanics. That adhesion is ~140 mJ/m^2 and independent of RH has been observed for silica glass [23], where the fracture plane is atomically smooth. The calculation and data are plotted as indicated in Fig. 5, and denoted "Calc #1". While the data from ref. [23] and calculation agree for a smooth interface, we conclude that the assumption of a smooth interface for polysilicon beams is poor, and that roughness must be considered. This is necessary because r_K is on the order of one nm, in spite of the 2.5 nm rms roughness reported above.

In the second model, we allow for roughness at the interface by considering capillary condensation at an asperity point as in Fig. 7. Because the radius of asperity tips R is large compared to r_K, the interfacial energy per wetted asperity contact can be shown to be [24]

$$W_{Asp} = 8\pi\gamma R\, r_K, \tag{6}$$

We make a first order assessment of Eq. (6). From AFM measurements, we obtain an approximate value of R=50 nm. Calling the asperity contact density n_{Asp} , inserting R=50 nm in Eq. (6) and substituting in Eq. (3), we obtain

$$\Gamma \approx W_{Asp} n_{Asp} = -n_{Asp} \frac{0.94\text{X}10^{-16}}{\ln(\text{RH})} \frac{\text{J}}{\text{m}^2}. \tag{7}$$

This relation is likewise plotted and labeled as "Calc #2" in Fig. 5, assuming n_{Asp}=20 per μm^2. Eq. (7) predicts that the adhesion is approximately exponential with RH, similar to the data. Between 30 and 80% RH, the slope for the data is perhaps somewhat greater than Eq. (7). This may be because in reality n_{Asp} likely increases as RH increases, due to the increasing Laplace pressure.

The effect of roughness on real contact area has long been recognized [25]. Tian and Bhushan [26] have recently implemented 3-D finite element modeling of rough surfaces brought into contact under humidified conditions. The rough surfaces were measured by AFM and directly inserted into the model. Their calculations indicate that the simple linear relationship between meniscus area and height does not exist for rough contacts. The value for n_{Asp} can perhaps be explained by studying the details of the manner in which rough surfaces come together.

SUMMARY AND CONCLUSIONS

We have studied the effect of RH on adhesion for hydrophilic polysilicon beams under equilibrium conditions. The data demonstrates that adhesion increases exponentially with RH. The analysis indicates that we can employ a single asperity model to understand the effect of RH on adhesion. These data and modeling improve our fundamental understanding of adhesion (e.g., stiction) in MEMS, and can lead to model-based calculations for MEMS design and packaging technology.

ACKNOWLEDGMENTS

Sandia National Laboratories is a multiprogram laboratory operated by Sandia Corporation, a Lockheed-Martin Company, for the United States Department of Energy under Contract DE-AC04-94AL85000. We thank J. M. Redmond for help in deriving Eq. (5), M. T. Dugger for obtaining the AFM data, and the staff at the Microelectronics Development Laboratory at Sandia National Laboratories for preparing the samples.

REFERENCES

1. C. H. Mastrangelo and C. H. Hsu, Proc. IEEE Solid-State Sensor & Actuator Workshop (Hilton Head) , 208 (1992).
2. C. H. Mastrangelo and C. H. Hsu, J. MEMS **2** (1), 33 (1993).
3. C. H. Mastrangelo and C. H. Hsu, J. MEMS **2** (1), 44 (1993).
4. M. P. de Boer and T. A. Michalske, Mater. Res. Soc. Proc. **444**, (1997).
5. M. P. de Boer and T. A. Michalske, J. Appl. Phys. , (to be submitted).
6. R. L. Alley, G. J. Cuan, R. T. Howe and K. Komvopoulos, Proc. IEEE Solid-State Sensor & Actuator Workshop (Hilton Head) , 202 (1992).
7. K. Deng, R. J. Collins, M. Mehregany and C. N. Sukenik, J. Electrochem. Soc. **142** (4), 1278 (1995).
8. B. P. Gogoi and C. H. Mastrangelo, J. MEMS **4** (4), 185 (1995).
9. R. L. Alley, P. Mai, K. Komvopoulos and R. T. Howe, Proc. Int. Conf. Solid-State Sensors & Actuators (Transducers '93) , 288 (1993).
10. M. R. Houston, R. Maboudian and R. T. Howe, Proc. IEEE Solid-State Sensor & Actuator Workshop (Hilton Head) , 42 (1996).
11. C. H. Mastrangelo and G. S. Saloka, Proc. IEEE MEMS (Ft. Lauderdale) , 77 (1993).
12. U. Srinivasan, M. R. Houston, R. T. Howe and R. Maboudian, Proc. Int. Conf. Solid-State Sensors & Actuators (Transducers '97) **2**, 1399 (1997).
13. Y. Yee, K. Chun and J. D. Lee, Proc. Int. Conf. Solid-State Sensors & Actuators (Transducers '95) , 206 (1995).
14. G. T. Mulhern, D. S. Soane and R. T. Howe, Proc. Int. Conf. Solid-State Sensors & Actuators (Transducers '93) , 296 (1993).
15. E. M. Russick, C. L. J. Adkins and C. W. Dyck, in *Supercritical Fluids, Extraction and Pollution Prevention,* M. A. Abraham and A. K. Sunol, ed. (American Chemical Society, Washington, DC, 1997), vol. 670, pp. 255-269.
16. M. R. Houston, R. T. Howe and R. Maboudian, J. Appl. Phys. **81** (8), 3474 (1997).
17. H. L. Ewalds and R. J. H. Wanhill, *Fracture Mechanics*, 82-84 (Edward Arnold and Delftse Uitgevers Maatschapij, London, 1991).
18. E. Garcia and J. Sniegowski, Sensors and Actuators A **48**, 203 (1995).
19. LabVIEW, National Instruments, Austin, TX, 78730, http://www.natinst.com/.
20. Analysis performed on using the public domain NIH image program, available from the NIH Image Web site (http://rsb.info.nih.gov/nih-image/).
21. H. Naono, R. Fujiwara and M. Yagi, J. Colloid Interface Sci. **76** (1), 74 (1980).
22. A. W. Adamson, *Physical Chemistry of Surfaces*, (John Wiley & Sons, New York, 1990).
23. T. A. Michalske and E. R. Fuller, J. Am. Ceram. Soc. **68** (11), 586 (1985).
24. J. Israelachvili, *Intermolecular and Surface Forces*, (Academic Press, New York, 1992).
25. J. A. Greenwood and J. B. P. Williamson, Proc. Roy. Soc. Lond. A. **295**, 300 (1966).
26. X.F. Tian and B. Bhushan, J. Phys. D. Appl. Phys **29** (1), 163 (1996).

Report Number (14) SAND--98-1034C
CONF-980405--

Publ. Date (11) 19980504
Sponsor Code (18) DOE/MA, XF
UC Category (19) UC-900, DOE/ER

DOE